Dislocation loops as a mechanism for thermoelectric power factor enhancement in silicon nano-layers

This manuscript was accepted by Appl. Phys. Lett. Click here to see the version of record.

Dislocation Loops as a Mechanism for Thermoelectric Power Factor Enhancement in Silicon Nano-Layers

Nick S. Bennett [a*], *Daragh Byrne* [b], *Aidan Cowley* [c], *Neophytos Neophytou* [d]

[a] Nano-Materials Lab., Institute of Mechanical, Process & Energy Engineering, School of Engineering & Physical Sciences, Heriot-Watt University, Edinburgh EH14 4AS, United Kingdom

[b] School of Physical Science, Dublin City University, Glasnevin, Dublin 9, Ireland

[c] European Astronaut Centre (EAC), European Space Agency (ESA), Linder Höhe, D-51147 Cologne, Germany

[d] School of Engineering, University of Warwick, Coventry CV4 7AL, United Kingdom

[*] Corresponding author, E: n.bennett@hw.ac.uk, T: +44 131 451 4379, F: +44 131 451 3129

A more than 70% enhancement in the thermoelectric power factor of single-crystal silicon is demonstrated in silicon nano-films, a consequence of the introduction of networks of dislocation loops and extended crystallographic defects. Despite these defects causing reductions in electrical conductivity, carrier concentration and carrier mobility, large corresponding increases in the Seebeck coefficient and reductions in thermal conductivity lead to a significant net enhancement in thermoelectric performance. Crystal damage is deliberately introduced in a sub-surface nano-layer

This manuscript was accepted by Appl. Phys. Lett. Click here to see the version of record.

within a silicon substrate, demonstrating the possibility to tune the thermoelectric properties at the nano-scale within such wafers in a repeatable, large-scale and cost-effective way.

The recent global drive to be more efficient in the way we use energy, particularly to reduce the amount of energy that goes to waste, has led to renewed interest in thermoelectrics (TE) for waste heat harvesting. In particular demand are materials that use elements that are less costly, less toxic and more Earth-abundant than the popular TE material bismuth telluride (Bi_2Te_3). Despite requiring the scarce element tellurium, Bi_2Te_3 has significantly better thermoelectric performance than more abundant elemental semiconductors, such as silicon (Si). Three material properties determine this performance – thermal conductivity (κ), Seebeck coefficient (S) and electrical conductivity (σ). These interlinked properties are commonly combined to describe performance in terms of the thermoelectric figure-of-merit (Z), where $Z = S^2\sigma/\kappa$. Bi_2Te_3 has approximately 100-fold better Z than bulk Si [1], but is approximately 30-times more expensive [2]. Therefore developing methods that provide significant gains in the Z of Si offers a potential route to more cost-effective and environmentally friendly thermoelectric devices.

Since highly-doped Si (doping ~10^{19} cm^{-3}) possesses S and σ competitive with other TE materials, much recent focus has been on reducing its thermal conductivity, which is too high for most practical applications. It been demonstrated possible via nano-structuring, to vastly reduce κ with little or no degradation of other parameters in structures such as Si nanowires, nanofilms or films containing porosity, periodic voids or vacancies [3-13]. This allows for higher Z and makes nano-structured Si an attractive TE material. Such findings, with variations, have been corroborated by numerous groups worldwide, through both theoretical and experimental studies [3-13].

This manuscript was accepted by Appl. Phys. Lett. Click here to see the version of record.

Due to this drastic reduction in κ, which is quickly reaching the amorphous limit, further improvements might come from Si's thermoelectric power factor ($PF = S^2\sigma$), for which to date limited progress has been made. However, a small set of recent studies have demonstrated that a significant improvement in Si's *PF* is sometimes possible for polycrystalline Si [14-16] where built-in potential barriers are created by nano-scale grain boundaries or voids [17], combined with high levels of doping. These potential barriers increase energy filtering and as a consequence, the Si Seebeck coefficient. Our previous work demonstrated that a Seebeck coefficient improvement is also realizable in single-crystal Si nanowires by the introduction of dislocation loops, which also create potential barriers and produce a similar effect [18]. This was so far only demonstrated in n-type material and for relatively lowly-doped Si, where the *PF* is far too low for practical applications.

In this current article we report that a significant enhancement in the power factor is also possible for p-type bulk material, and more importantly, with high doping concentrations. Improvements in the *PF* by ~70 % compared to control samples (bulk Si) are realized, giving $PF = 6.6$ mW m^{-1} K^{-2} at 300 K – significantly higher than that of traditional Bi_2Te_3 materials used in current commercial devices.

Four different sample types were fashioned from prime <100> single-crystal Si wafers (n-type, 5-10 Ω cm). Ion-implantation of ^{28}Si ions was carried out on a Varian VIISta ion implanter at beam energy 2 MeV. Two wafers received a fluence of 2×10^{15} ions cm^{-2} and two others received 6×10^{15} ions cm^{-2}. Wafers received thermal annealing in nitrogen in a furnace at 900°C for a time of either 20 or 60 mins, before being diced into squares. Along with a non-implanted control wafer, samples were then thinned by etching in 25% KOH solution at 60°C, to precisely remove the top 1.5 μm of the wafer. Spin-on dopant (boron) was deposited on each sample before heating

This manuscript was accepted by Appl. Phys. Lett. Click here to see the version of record.

for 10 mins at 900°C in nitrogen to drive-in the dopant, creating a p-type region with a p/n junction immediately beneath it, isolating the p-type defect-rich nano-layer from the n-type substrate. A dip in HF was applied to remove surface boron-silicate glass. The B doping profile was confirmed as being the same in all samples by differential Hall profiling [19], with a relatively flat doping peak. This confirmed the junction depth as being ~800 nm, to coincide with the bottom of the defective layer and that the thickness of pristine Si remaining at the top of the film was only ~30-45 nm. Fig. 1 provides a schematic illustration of the steps used for sample fabrication.

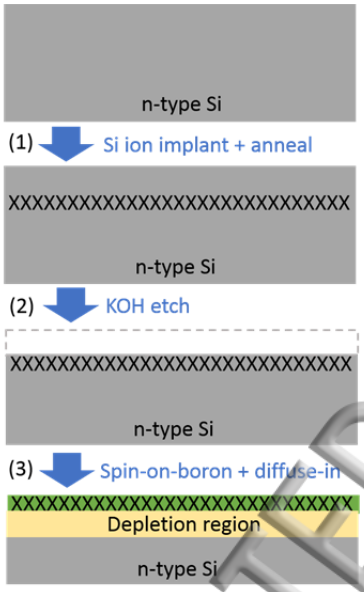

Figure 1. Schematic diagram showing the sample fabrication steps. The Si wafers underwent Si ion-implantation and annealing to create a sub-surface nano-layer rich in defects (represented by Xs). Following removal of the wafer surface by KOH etching, the nano-layer was doped p-type, creating a p/n junction and isolating it from the n-type substrate.

Each sample underwent characterization. The presence and nature of defects in the nano-layers were characterized by cross-sectional transmission electron microscopy (XTEM). Micrographs of each of the samples created are presented in Fig. 2. Fig. 2(a) shows the location of the buried

layer relative to the original wafer surface. The remaining micrographs show shows defects created with each of the four implant/annealing conditions. All micrographs show clear evidence of dislocation loops and implantation extended defects, with the higher implant dose creating a higher density of defects. Samples were sent to a commercial vendor for through-plane thermal conductivity measurements. These were extracted by a thermo-reflectance method. Electrical conductivity, Hall-effect and differential Hall measurements were made in air in van der Pauw geometry, using a Biorad HL5900 tool. Temperature-dependent electrical conductivity and Seebeck measurements were made in-plane on a Linseis LSR-3 instrument in He ambient at 10^4 Pa.

This manuscript was accepted by Appl. Phys. Lett. Click here to see the version of record.

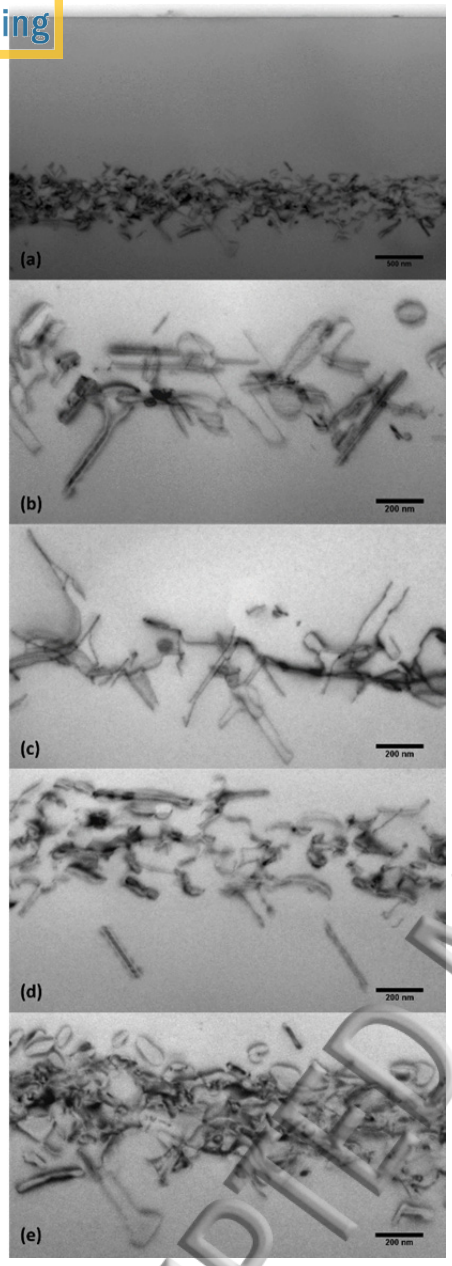

Figure 2. Micrographs showing sub-surface defect-rich regions created in the Si wafers. (a) Shows the layer location relative to the wafer surface (scale bar is 500 nm). (b) Shows defects created with 2 x 10^{15} cm^{-2} implant, 900°C, 20 mins annealing. (c) Shows defects created with 2 x 10^{15} cm^{-2} implant, 900°C, 60 mins annealing. (d) Shows defects created with 6 x 10^{15} cm^{-2} implant, 900°C, 20 mins annealing. (e) Shows defects created with 6 x 10^{15} cm^{-2} implant, 900°C, 60 mins annealing. (Scale bars in (b)-(e) are 200nm).

This manuscript was accepted by Appl. Phys. Lett. Click here to see the version of record.

Fig. 3 shows the variation with implant/annealing conditions for through-plane thermal conductivity at 300 K. κ was 132.6 W m^{-1} K^{-1} for the defect-free control sample and was found to decrease significantly as a result of implantation-induced damage. κ fell to a value of 70.4 W m^{-1} K^{-1} for the lower implantation fluence with 20 min annealing, but recovered slightly to 76.6 W m^{-1} K^{-1} following annealing for 60 min. This was an expected result since it is both intuitive and well-established that the introduction of defects within a 'perfect' crystal lattice reduces its thermal transport, and that with longer annealing, more damage will be removed and recovery of thermal transport will occur. For the larger fluence, κ was reduced more, to 43.2 W m^{-1} K^{-1} for 20 min annealing and to 48.9 W m^{-1} K^{-1} with 60 min annealing.

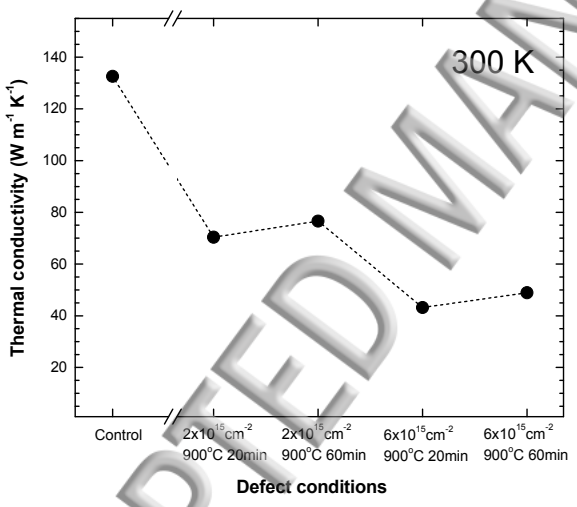

Figure 3. Thermal conductivity (through-plane) as a function of implant/annealing conditions for a control sample relative to samples with 2 MeV Si implant with (i) 2 x 10^{15} cm^{-2} fluence, 900°C, 20 mins annealing, (ii) 2 x 10^{15} cm^{-2} fluence, 900°C, 60 mins annealing, (iii) 6 x 10^{15} cm^{-2} fluence, 900°C, 20 mins annealing, and (iv) 6 x 10^{15} cm^{-2} fluence, 900°C, 60 mins annealing. Measurements were made at 300 K.

Fig. 4 shows the change in σ in each sample as a function of the conditions used to create defects. Results are displayed for measurements made at 300, 350 and 400 K, although

This manuscript was accepted by Appl. Phys. Lett. Click here to see the version of record.

differences as a result of temperature were modest in these samples, with only a small conductivity decrease seen in each sample as the measurement temperature is raised. More obvious was the change in conductivity as the implant/annealing conditions were changed. Clearly the control sample had the highest σ of 415 S cm^{-1}. For the lower of the implant fluences, conductivity was reduced relative to the control, and for the higher fluence, conductivity was reduced to less than half. For each fluence, it was the sample that received the shortest anneal that had the lowest conductivity. These trends are intuitive and it is unsurprising that trends in electrical conductivity match those in thermal conductivity (Fig. 3). These trends are similar in magnitude, i.e. as thermal conductivity is reduced for a given condition, so is electrical conductivity by a similar extent, suggesting little net gain in electrical/thermal transport behavior results from the introduction of dislocations, each quantity being reduced by a factor of ~3. It is worth mentioning that XTEM images – particularly Fig. 2(d) and 2(e) – are perhaps deceiving, as one might expect the electrical/thermal conductivity to be lower for the sample in Fig. 2(e) where defects are more apparent. This is opposite to what is measured. In reality, samples having received shorter anneals contain the most defects and lower electrical/thermal conductivity, yet these defects are in the form of smaller Si-interstitial clusters, not visible in the XTEM at its current resolution.

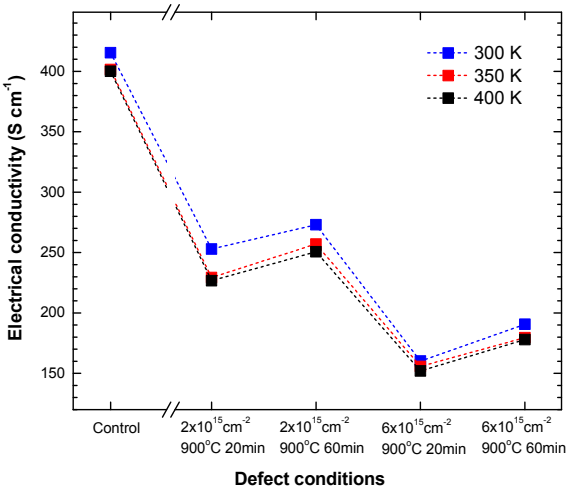

131

132 **Figure 4.** Electrical conductivity (in-plane) as a function of ion-implantation condition and annealing time, for three
133 measurement temperatures (300 K - 400 K).

134 Fig. 5 gives further detail of the room-temperature σ by way of Hall measurement data. Carrier
135 concentration and Hall mobility at 300 K are presented. They show that defect-mediated
136 decreases in σ are a result of a fall in both Hall mobility and carrier concentration, though the
137 former drop is more significant. Crystallographic defects are well known to degrade carrier
138 mobility in Si and this clearly occurs in current samples. B dopant activation is highest in the
139 control sample following drive-in, whereas defects reduce the carrier concentration by up to
140 10%. Since B is well-known to cluster with self-interstitials it is likely that their presence during
141 the drive-in phase means a proportion of the dopants are trapped in inactive clusters rather than
142 finding substitutional sites. B activation improves slightly after longer-duration annealing.

This manuscript was accepted by Appl. Phys. Lett. Click here to see the version of record.

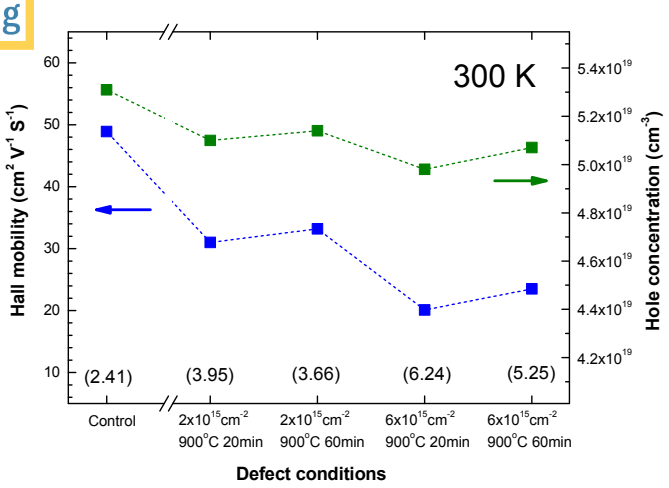

Figure 5. Hall mobility (left axis) and hole concentration (right) as a function of defect conditions. Measurements were made at 300 K. Values in parentheses are corresponding resistivity values in mΩ cm.

In-plane Seebeck coefficient measurements were carried out for each of the samples. Results are displayed for measurements made at 300, 350 and 400 K, although as for σ, temperature-dependent differences are modest, with only a small S increase seen in each sample as the measurement temperature is raised. In this case S was lowest in the control sample (Fig. 6(a)), though this was expected since that sample had the highest electrical conductivity and the two parameters are interrelated, with one usually increasing at the expense of the other. Combining the two in the form of the power factor gives an indication of the net thermoelectric performance, with $PF = 3.8$ mW m^{-1} K^{-2} at 300 K for the control sample (Fig. 6(b)). This PF value is in line with the highest value pristine Si can provide under optimal doping conditions. All other samples, with lower electrical conductivity, have a higher Seebeck coefficient. The two samples receiving the lower implant dose (2x10^{15} cm^{-2}) have modestly higher S that, when combined with σ, result in a significantly lower thermoelectric PF than the control sample. For the higher implant fluence (6x10^{15} cm^{-2}) with 20 min annealing the PF is worse still, since the relatively

small rise in S is more than negated by the much larger drop in σ. An interesting result occurs however, when the higher fluence sample is annealed for longer, resulting in the formation of a dense network of mostly dislocation-loops with diameters roughly between 100 nm and 200 nm (Fig. 2(e)). In this case the increase in S is much greater than for all other samples and bucks the trend, since given its higher electrical conductivity than the previously mentioned sample, one would expect its Seebeck coefficient to decrease. In fact, as the reader can see, not only is the opposite true, but the increase in S is significant. This has a striking effect on the power factor, which is now on average 70% higher than that of the control sample, with PF = 6.6 mW m^{-1} K^{-2} at 300 K.

This manuscript was accepted by Appl. Phys. Lett. Click here to see the version of record.

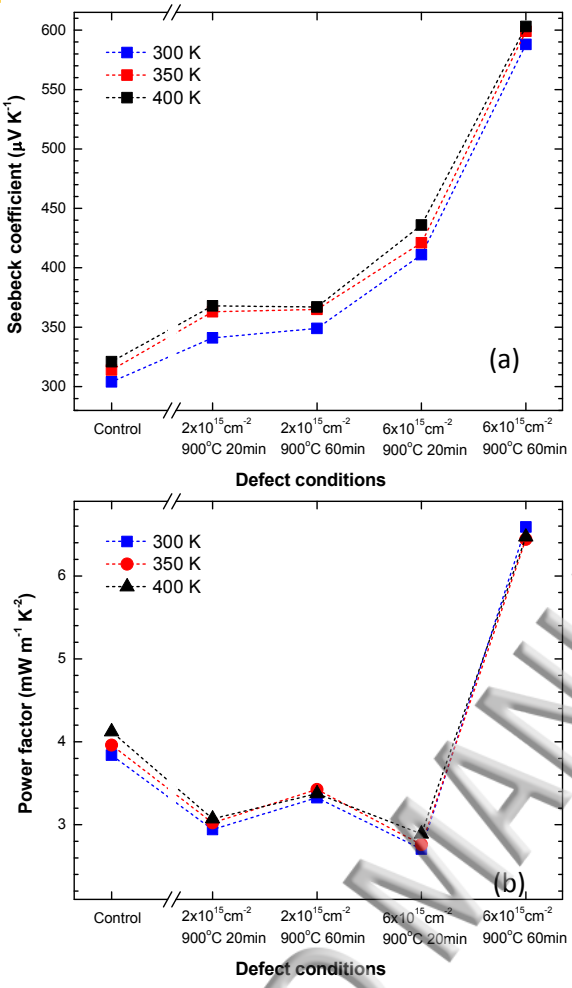

Figure 6. (a) Seebeck coefficient (in-plane) and (b) power factor as a function of defect conditions for three measurement temperatures (300 K - 400 K).

The simultaneous increase in σ and S is rare, but significant, and results in improved power factors. It is similar to that observed in reference [14] for heavily B-doped nano-crystalline Si, again under high-temperature annealing. While the underlying reasons behind this are still under investigation, it is possible that a number of contributing factors coexist and act synergistically in order to achieve a simultaneous S and σ improvement. For the former, it is probable that potential barriers for holes are created at the dislocation sites, which improve energy filtering and consequently S. Indeed, when present within the crystal lattice, dislocation loops are known to

This manuscript was accepted by Appl. Phys. Lett. Click here to see the version of record.

exert a significant pressure by pushing-apart nearby Si atoms – this pressure increasing the band-gap local to the dislocation site [20]. For the first annealing condition, this local band-gap increase could be responsible for the reduction in conductivity and mobility. As well as allowing loops to form, longer annealing would heal the majority of the Si volume, and thus a slight increase in the electrical conductivity is observed, compensating for any further reduction from the increasing potential barriers. The increased pressure may also improve carrier mobility, a well-known consequence of applying stress in Si [21]. In addition, any local thermal conductivity differences between pristine Si regions and the dislocations might improve *S* as well. This is because the overall Seebeck coefficient is determined by the weighted average of *S* in the two regions, with the weighting factor being the temperature drop in each region, determined by their thermal conductivities [14, 22]. Thus, as the crystal lattice is healed, especially in the last annealing step, and local thermal conductivity increases, the local Seebeck coefficient in the dislocation regions (which is expected to be high compared to bulk Si) becomes more important and could warrant the large increase in the overall *S* observed in Fig. 6(a). Our earlier calculations on the effect of filtering by barriers in p-type Si, indicate that filtering alone could provide ~30-40% *PF* improvements [22, 23], whereas the rest of the measured improvements could originate from the various other factors identified, such as local variations in thermal conductivity and carrier mobility.

We have reported a significant enhancement in the power factor of single-crystal Si is possible for highly-doped p-type material, specifically an improvement of ~70 % compared to control samples (bulk Si), giving $PF = 6.6$ mW m^{-1} K^{-2} at 300 K. This is higher than that of traditional Bi_2Te_3 materials used in commercial thermoelectric devices [24] and is a consequence of the introduction of a dense network of dislocation loops with diameter

between 100 nm and 200 nm. Despite these defects causing reductions in electrical conductivity, carrier concentration and carrier mobility, large corresponding increases in Seebeck coefficient and reductions in thermal conductivity lead to a significant net enhancement in thermoelectric performance. This finding provides a route to significant gains in the thermoelectric power factor of Si, a material that potentially offers a path to more cost-effective and environmentally-friendly thermoelectric devices.

Acknowledgements

NSB, DB and AC thank Science Foundation Ireland for partial support of this work through grant 12/TIDA/E2378 and the Royal Society for supporting research exchange through grant IE131212. NN acknowledges funding from the European Research Council (ERC) under the European Union's Horizon 2020 research and innovation programme (grant agreement No 678763). Dr Jan-Willem Bos of Heriot-Watt University is gratefully acknowledged for access to Seebeck measurement facilities.

References

[1] L. Weber and E. Gmelin, Transport properties of silicon. Appl. Phys. A 53 (1991) 136–140.

[2] S. Leblanc, S. K. Yee, M. L. Scullin, C. Dames, and K. E. Goodson, Material and manufacturing cost considerations for thermoelectrics, Renewable and Sustainable Energy Reviews 32 (2014) 313.

[3] A. I. Hochbaum, R. Chen, R. D. Delgado, W. Liang, E. C. Garnett, M. Najarian, A. Majumdar, and P. D. Yang, Enhanced thermoelectric performance of rough silicon nanowires, Nature 451 (2008) 163–167.

223 [4] A. I. Boukai, Y. Bunimovich, K. J. Tahir, J. Yu, W. A. Goddard, and J. R. Heath, Silicon
224 nanowires as efficient thermoelectric materials, Nature 451 (2008) 168–171.

225 [5] G. Pennelli, and M. Macucci, Optimization of the thermoelectric properties of nanostructured
226 silicon, J. Appl. Phys. 114 (2013) 214507.

227 [6] E. B. Ramayya, L. N. Maurer, A. H. Davoody, and I. Knezevic, Thermoelectric properties of
228 ultrathin silicon nanowires, Phys. Rev. B 86 (2012) 115328.

229 [7] I. Bejenari and P. Kratzer, Atomistic calculation of the thermoelectric properties of Si
230 nanowires, Phys. Rev. B 90 (2014) 045429.

231 [8] W. Liu, K. Etessam-Yazdani, R. Hussin, and M. Asheghi, Modeling and Data for Thermal
232 Conductivity of Ultrathin Single-Crystal SOI Layers at High Temperature. IEEE Transactions on
233 electron devices 53 (8) (2006) 1868.

234 [9] J. Tang, H. Wang, D. H. Lee, M. Fardy, Z. Huo, T. P. Russell, and P. Yang, Holey silicon as
235 an efficient thermoelectric material, Nano Lett. 10 (2010) 4279-4283.

236 [10] J.-K. Yu, S. Mitrovic, D. Tham, J. Varghese, and J. R. Heath, Reduction of thermal
237 conductivity in phononic nanomesh structures, Nature Nanotechnology 5 (2010) 718–721.

238 [11] P. E. Hopkins, C. M. Reinke, M. F. Su, R. H. Olsson III, E. A. Shaner, Z. C. Leseman, J. R.
239 Serrano, L. M. Phinney, and I. El-Kady, Reduction in the Thermal Conductivity of Single
240 Crystalline Silicon by Phononic Crystal Patterning, Nano Lett. 11 (2011) 107-112.

241 [12] B. Xu and K. Fobelets, Spin-on-doping for output power improvement of silicon nanowire
242 array based thermoelectric power generators, J. Appl. Phys. 115 (2014) 214306.

[13] N. S. Bennett, N. W. Wight, S. R. Popuri, and J.-W. G. Bos, Efficient thermoelectric performance in silicon nano-films by vacancy-engineering, Nano Energy 16 (2015) 350-356.

[14] N. Neophytou, X. Zianni, H. Kosina, S. Frabboni, B. Lorenzi, and D. Narducci, Simultaneous increase in electrical conductivity and Seebeck coefficient in highly Boron-doped nanocrystalline Si, Nanotechnology 24 (2013) 205402.

[15] N. Neophytou, X. Zianni, H. Kosina, S. Frabboni, B. Lorenzi, and D. Narducci, Power factor enhancement by inhomogeneous distribution of dopants in two-phase nanocrystalline systems, Journal of Electronic Materials 43 (6) (2014) 1896-1904.

[16] D. Narducci, B. Lorenzi, X. Zianni, N. Neophytou, S. Frabboni, G. C. Gazzadi, A. Roncaglia, and F. Suriano, Enhancement of the power factor in two-phase silicon-boron nanocrystalline alloys, Physica status solidi a 211 (6) (2014) 1255-1258.

[17] B. Lorenzi , D. Narducci, R. Tonini, S. Frabboni, G.C. Gazzadi, G. Ottaviani, N. Neophytou, X. Zianni, Paradoxical enhancement of the power factor in polycrystalline silicon due to the formation of nanovoids, Journal of Electronic Materials 43 (10) (2014) 3812-3816.

[18] N. S. Bennett, D. Byrne and A. Cowley, Enhanced Seebeck coefficient in silicon nanowires containing dislocations, Appl. Phys. Lett. 107 (2015) 013903.

[19] N. S. Bennett and N. E. B. Cowern, Doping characterization for germanium-based microelectronics and photovoltaics using the differential Hall technique, Appl. Phys. Lett. 100 (2012) 172106.

[20] K. P. Homewood and M. A. Lourenço, Light from Si via dislocation loops, Materials Today 8 (1) (2005) 34-39.

[21] M. L. Lee, E. A. Fitzgerald, M. T. Bulsara, M. T. Currie and A. Lochtefeld, Strained Si, SiGe, and Ge channels for high-mobility metal-oxide-semiconductor field-effect transistors, J. Appl. Phys. 97 (2005) 011101.

[22] R. Kim and M. S. Lundstrom, Computational study of energy filtering effects in one-dimensional composite nano-structures, J. Appl. Phys. 111 (2012) 024508.

[23] N. Neophytou and H. Kosina, Optimizing Thermoelectric Energy Filtering by Means of a Potential Barrier, J. Appl. Phys., 114 (2013) 044315.

[24] "Thermoelectric Energy Harvesting 2016-2026: Devices, Applications, Opportunities", IDTechEx Report by H. Zervos, updated June 2016, www.idtechex.com

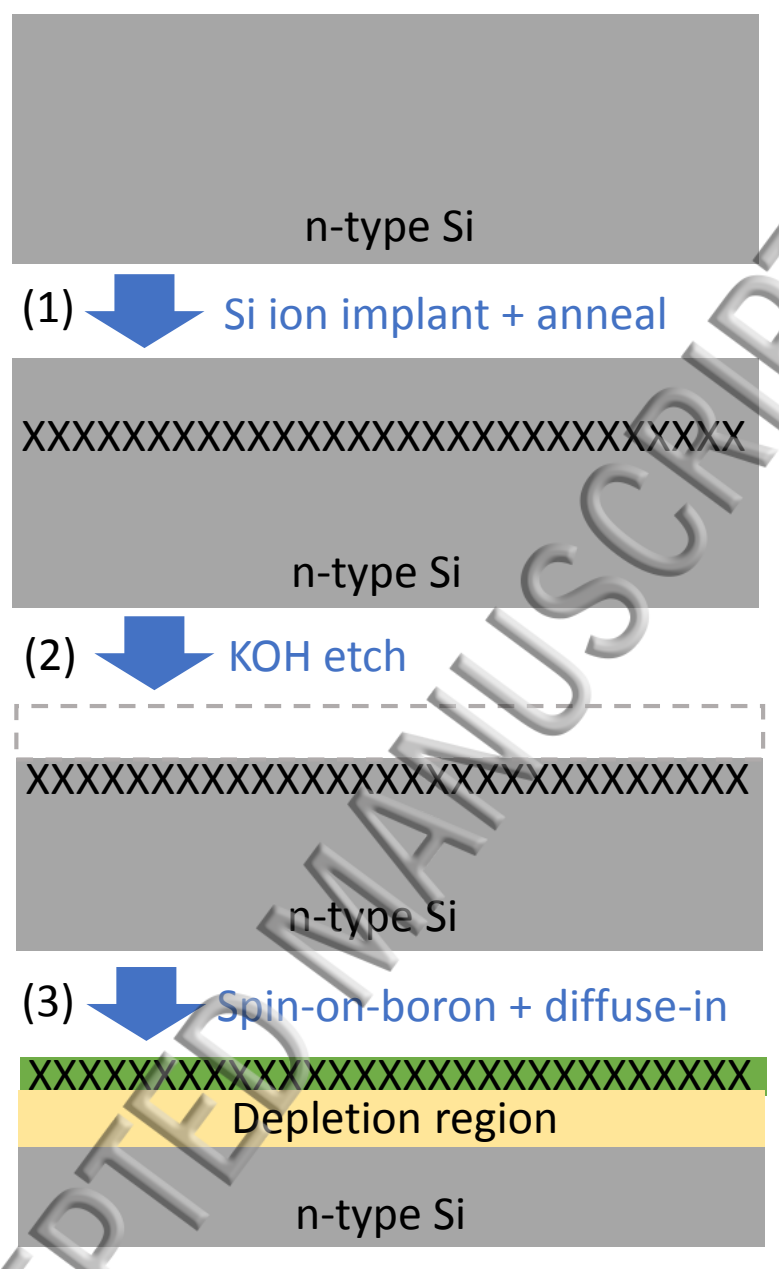

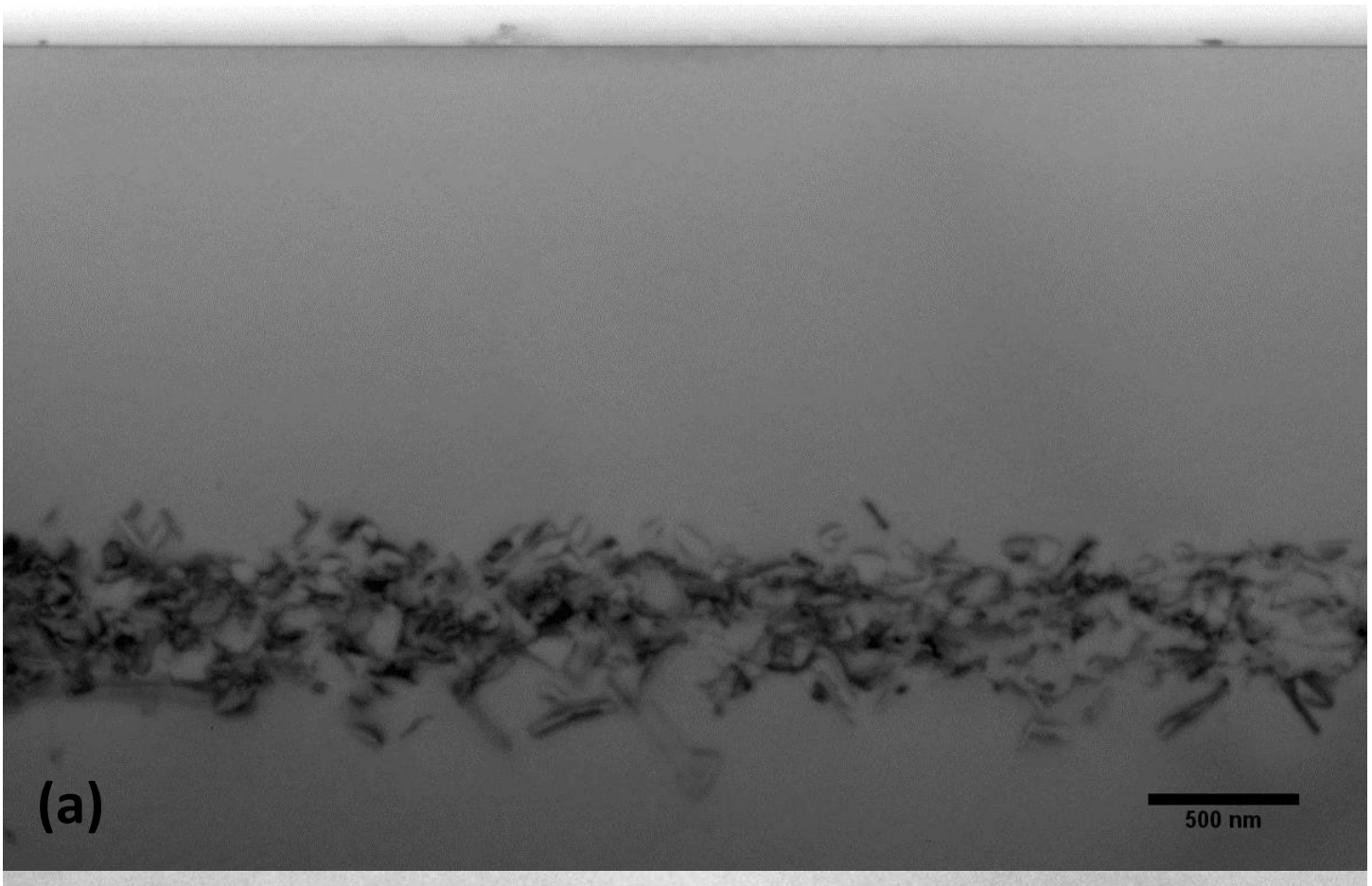

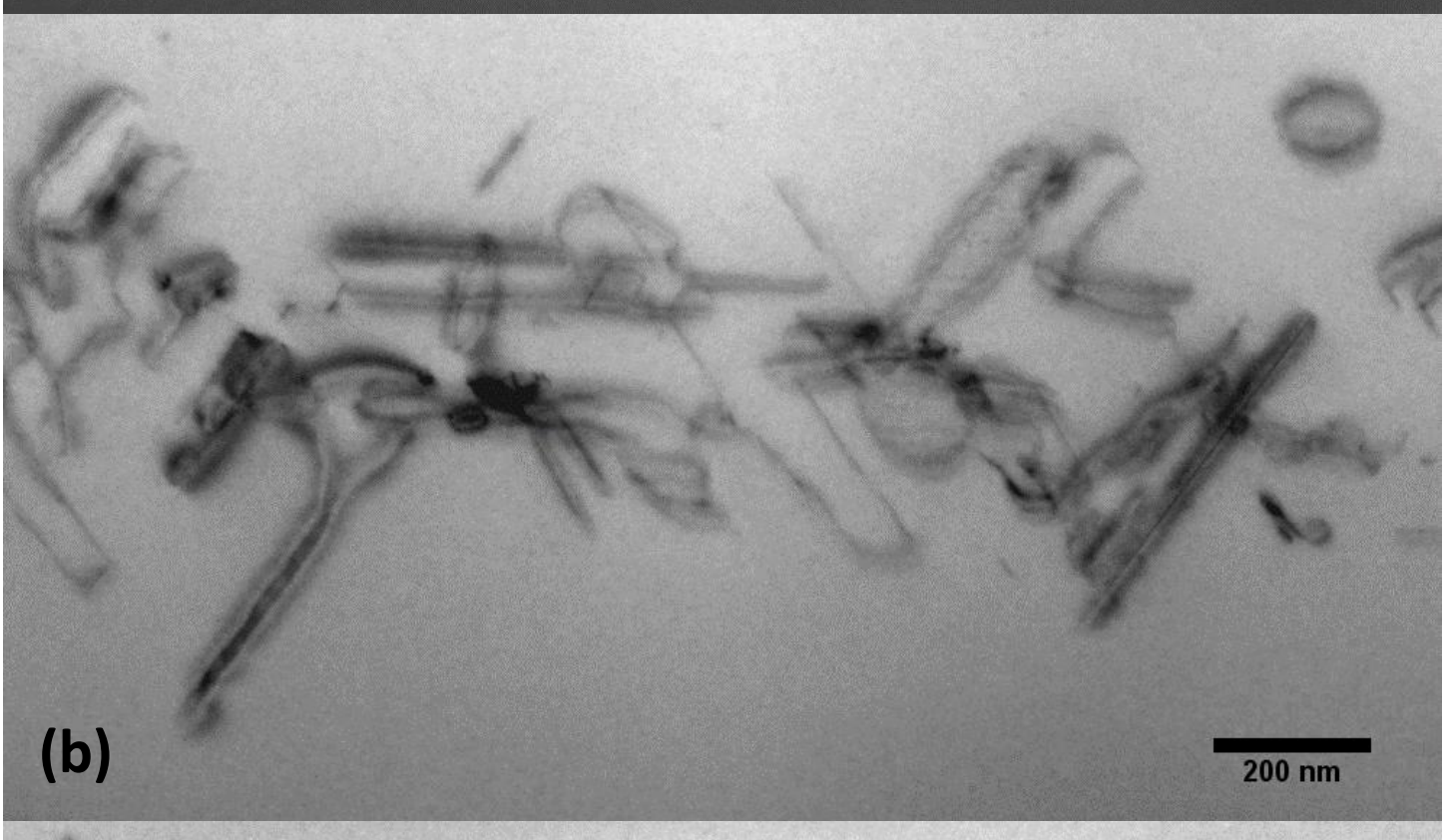

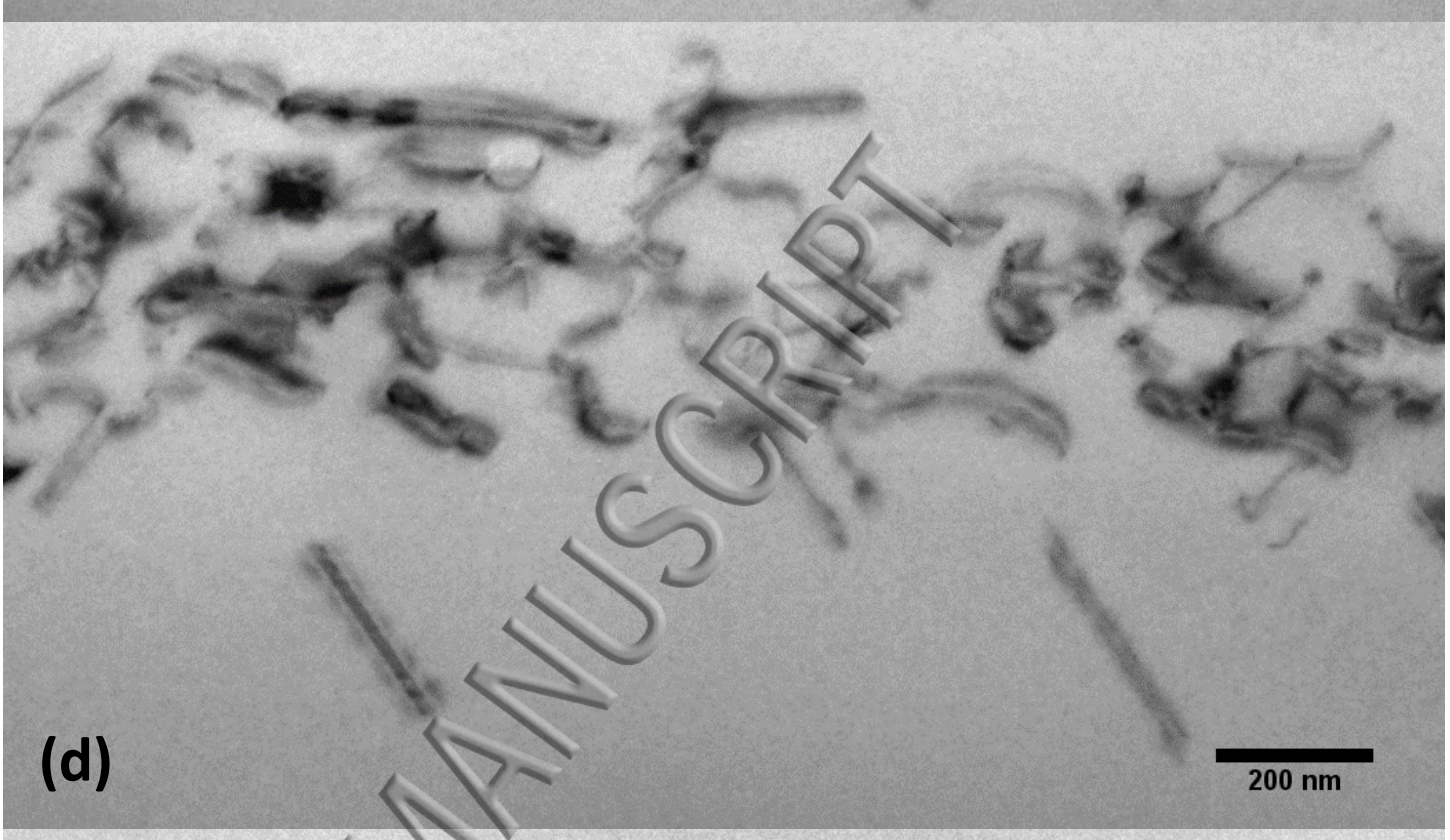

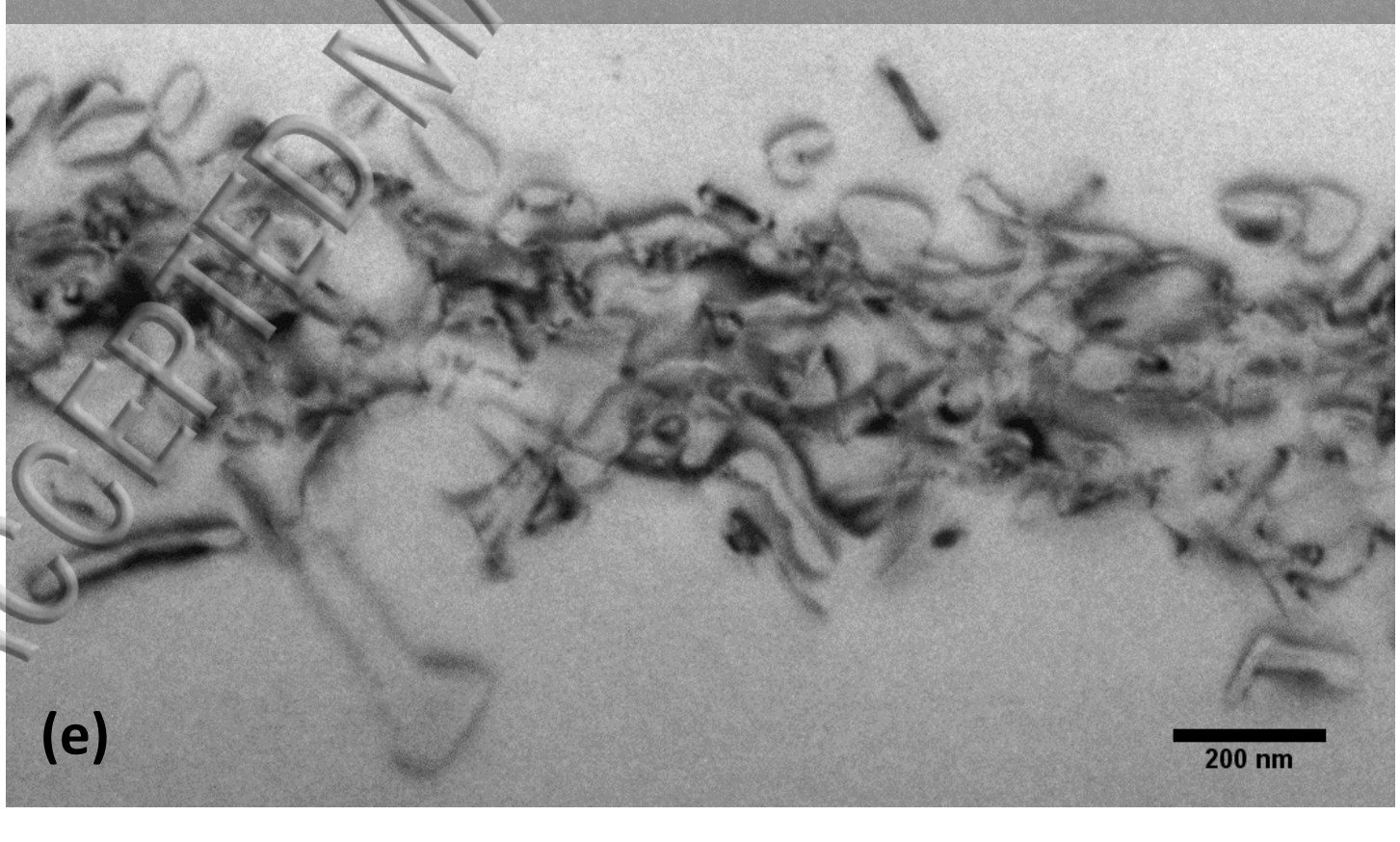

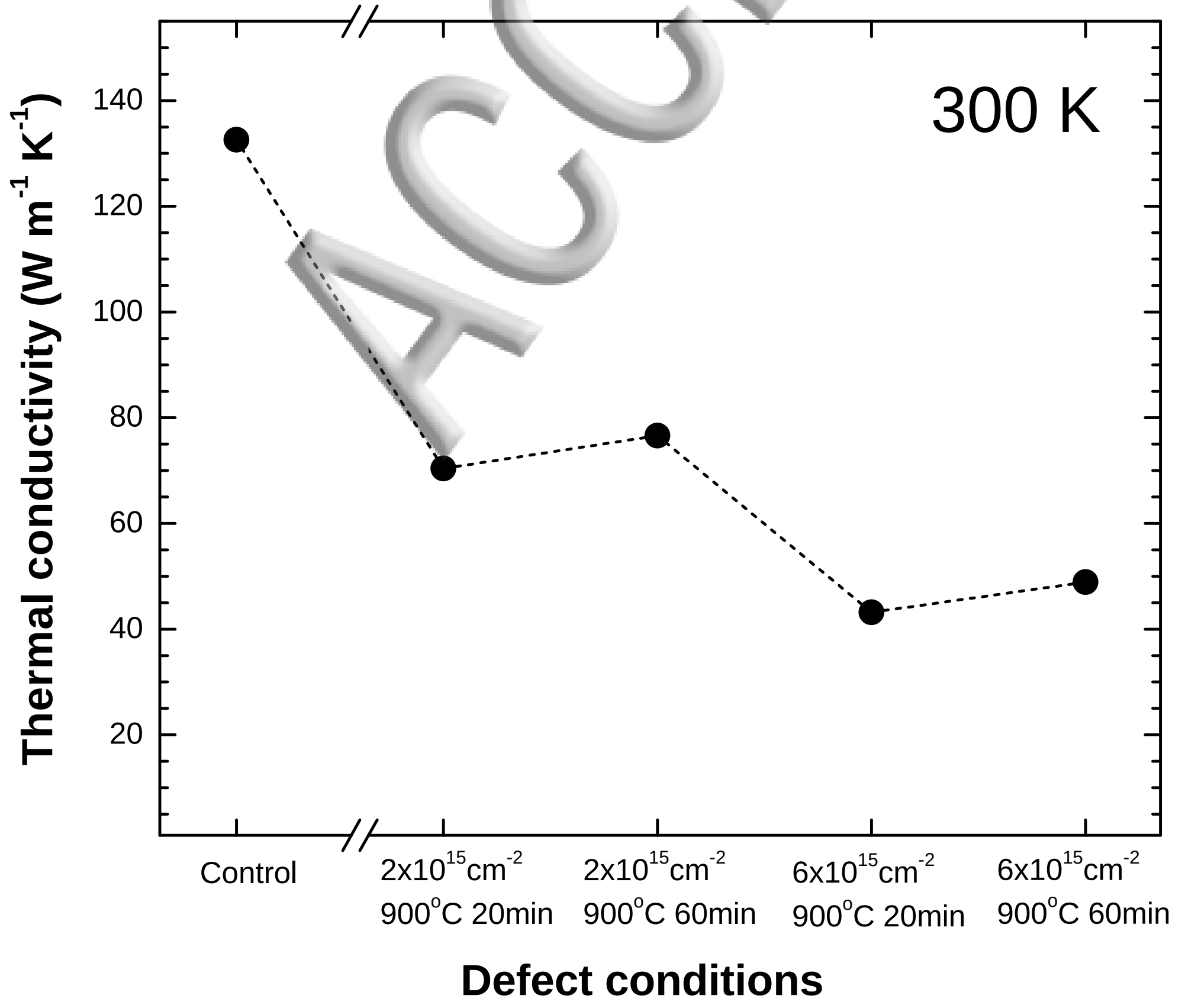
300 K
Thermal conductivity (W m-1 K-1)
140
120
100
80
60
40
20
Control
2x10^15cm^-2 900°C 20min
2x10^15cm^-2 900°C 60min
6x10^15cm^-2 900°C 20min
6x10^15cm^-2 900°C 60min
Defect conditions

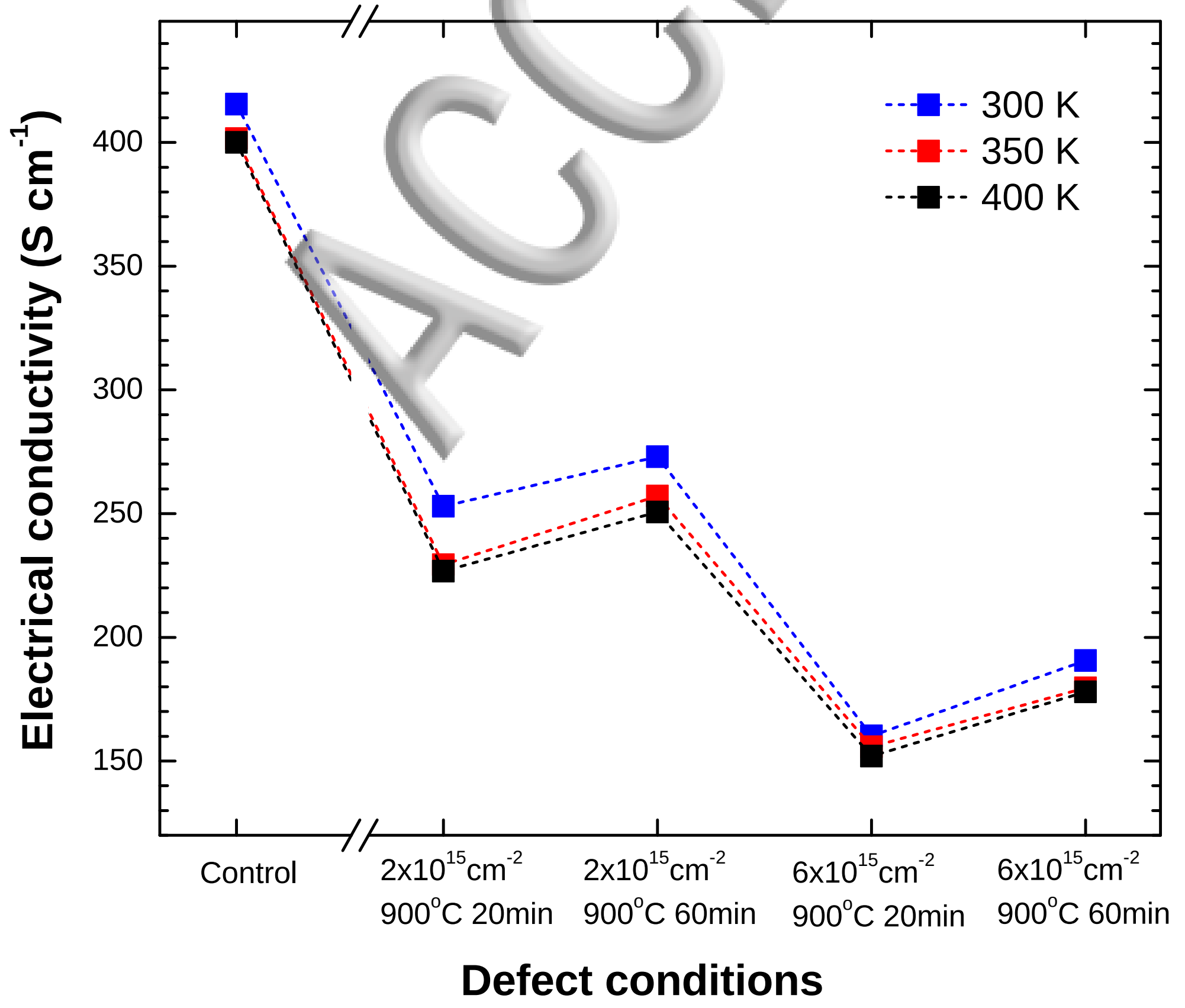
Electrical conductivity (S cm-1)
400
350
300
250
200
150
300 K
350 K
400 K
Control
2x10^15cm^-2 900°C 20min
2x10^15cm^-2 900°C 60min
6x10^15cm^-2 900°C 20min
6x10^15cm^-2 900°C 60min
Defect conditions

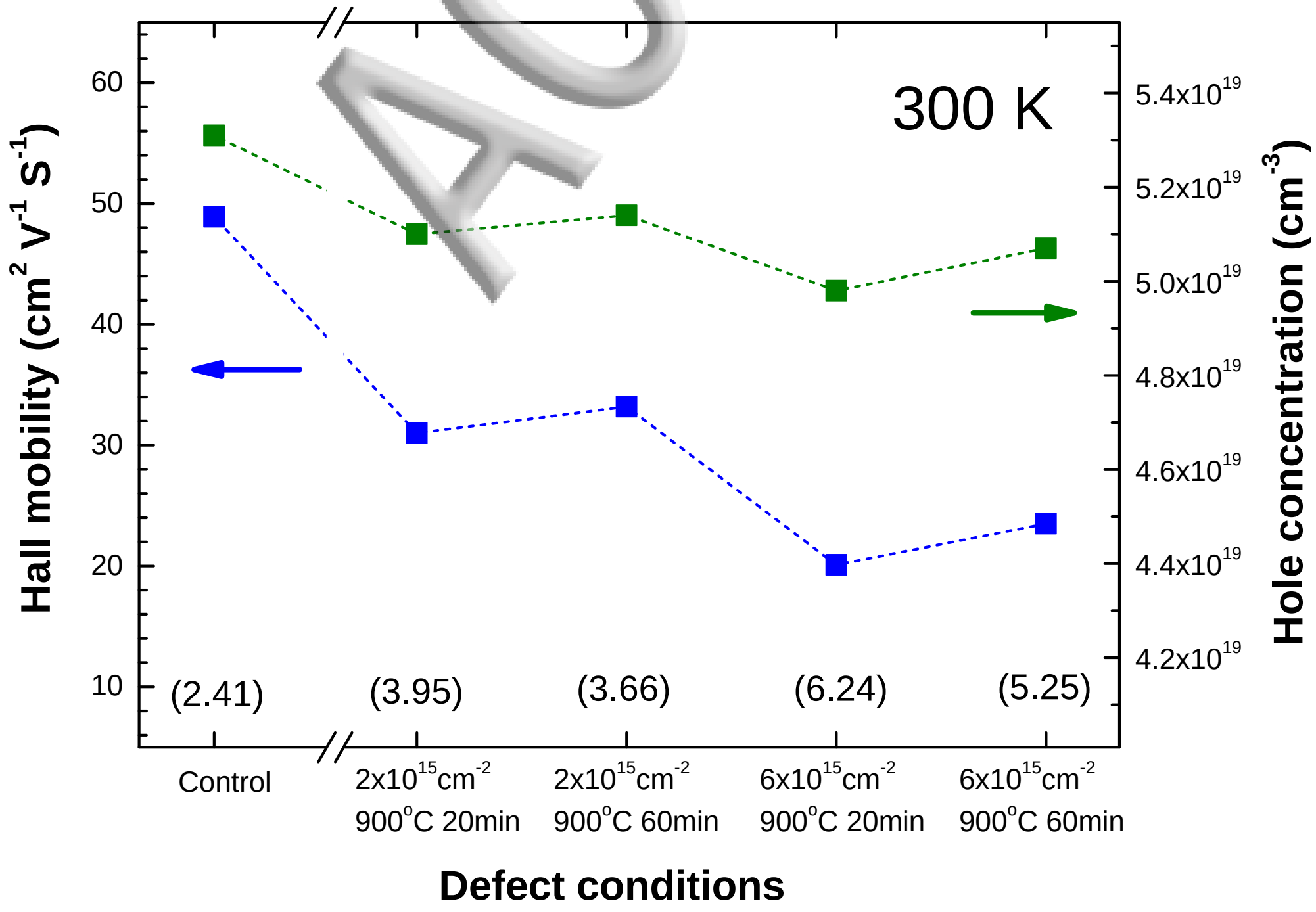
300 K
Hall mobility (cm^2 V^{-1} S^{-1})
Hole concentration (cm^{-3})
60
50
40
30
20
10
5.4x10^{19}
5.2x10^{19}
5.0x10^{19}
4.8x10^{19}
4.6x10^{19}
4.4x10^{19}
4.2x10^{19}
(2.41)
(3.95)
(3.66)
(6.24)
(5.25)
Control
2x10^{15}cm^{-2} 900^{o}C 20min
2x10^{15}cm^{-2} 900^{o}C 60min
6x10^{15}cm^{-2} 900^{o}C 20min
6x10^{15}cm^{-2} 900^{o}C 60min
Defect conditions

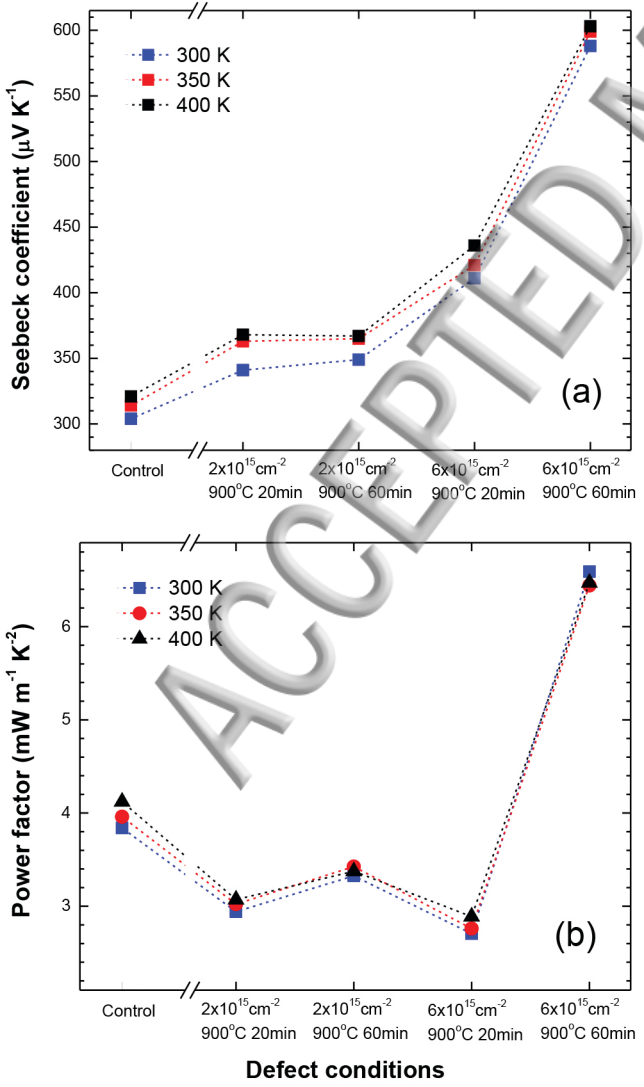
300 K
350 K
400 K
Seebeck coefficient (μV K-1)
(a)
Control
2x10^15cm^-2 900°C 20min
2x10^15cm^-2 900°C 60min
6x10^15cm^-2 900°C 20min
6x10^15cm^-2 900°C 60min
300 K
350 K
400 K
Power factor (mW m-1 K-2)
(b)
Control
2x10^15cm^-2 900°C 20min
2x10^15cm^-2 900°C 60min
6x10^15cm^-2 900°C 20min
6x10^15cm^-2 900°C 60min
Defect conditions